

# Less noticeable shallow decay phase in early X-ray afterglows of GeV/TeV-detected gamma-ray bursts

Ryo Yamazaki,<sup>1,2\*</sup> Yuri Sato<sup>1</sup>, Takanori Sakamoto<sup>1</sup>, Motoko Serino<sup>1</sup>

<sup>1</sup>*Department of Physics and Mathematics, Aoyama Gakuin University, 5-10-1 Fuchinobe, Sagamihara 252-5258, Japan*

<sup>2</sup>*Institute of Laser Engineering, Osaka University, 2-6 Yamadaoka, Suita, 565-0871 Osaka, Japan*

## ABSTRACT

The nature of the shallow decay phase in the X-ray afterglow of the gamma-ray burst (GRB) is not yet clarified. We analyze the data of early X-ray afterglows of 26 GRBs triggered by Burst Alert Telescope onboard *Neil Gehrels Swift Observatory* and subsequently detected by *Fermi* Large Area Telescope (LAT) and/or Imaging Atmospheric Cherenkov Telescopes. It is found that 9 events (including 2 out of 3 very-high-energy gamma-ray events) have no shallow decay phase and that their X-ray afterglow light curves are well described by single power-law model except for the jet break at later epoch. The rest are fitted by double power-law model and have a break in the early epoch (around ks), however, 8 events (including a very-high-energy gamma-ray event) have the pre-break decay index larger than 0.7. We also analyze the data of well-sampled X-ray afterglows of GRBs without LAT detection, and compare their decay properties with those of high-energy and very-high-energy gamma-ray events. It is found that for the GeV/TeV bursts, the fraction of events whose X-ray afterglows are described by single power-law is significantly larger than those for non GeV/TeV GRBs. Even if the GeV/TeV GRBs have shallow decay phase, their decay slope tends to be steeper than non GeV/TeV bursts, that is, they have less noticeable shallow decay phase in the early X-ray afterglow. A possible interpretation along with the energy injection model is briefly discussed.

**Key words:** (transients:) gamma-ray bursts — (stars:) gamma-ray burst: general

## 1 INTRODUCTION

X-ray afterglows of gamma-ray bursts (GRBs) are not fully understood as of yet (see, e.g., Kumar & Zhang 2015, for review). Their canonical behavior consists of the initial steep decay phase, the shallow decay phase and the normal decay phase (Nousek, et al. 2006; Zhang, et al. 2006), which is subsequently followed by the steepening again due to the jet break (Liang, et al. 2008; Racusin, et al. 2009). The initial steep decay phase is most likely the tail emission of the prompt GRB (Kumar & Panaitescu 2000; Zhang, et al. 2006; Yamazaki, et al. 2006), and the late normal decay phase is well explained by the external forward shock model proposed in the pre-*Swift* era (Sari, Piran & Narayan 1998). The most enigmatic is the shallow decay phase which typically lasts  $10^3$ – $10^4$  s (Willingale, et al. 2007; Liang, Zhang & Zhang 2007; Sakamoto, et al. 2008; Dainotti, et al. 2010, 2013, 2016; Margutti, et al. 2013; Tang et al. 2019; Zhao et al. 2019). Proposed models are the energy injection model

(Nousek, et al. 2006; Zhang, et al. 2006; Granot & Kumar 2006; Kobayashi & Zhang 2007), the inhomogeneous or two-component jet model (Toma, et al. 2006; Eichler & Granot 2006; Granot, Königl & Piran 2006; Beniamini et al. 2020), the time-dependent microphysics model (Ioka, et al. 2006; Granot, Königl & Piran 2006; Fan & Piran 2006), the prior explosion model (Ioka, et al. 2006; Yamazaki 2009), the cannonball model (Dado, Dar & De Rújula 2006), the reverse-shock-dominated afterglow model (Genet, Daigne & Mochkovitch 2007), the internal engine model (Ghisellini, et al. 2007), the supercritical pile model (Sultana, Kazanas & Mastichiadis 2013), the collapsar model ejecting thick shells (van Eerten 2014), the high-latitude emission from structured jets (Oganesyan, et al. 2019) and so on. To clarify the mechanism of the shallow decay phase, additional observational information other than X-rays is necessary.

High-energy gamma-ray emissions are detected by *Fermi* Large Area Telescope (LAT) either during or after the prompt GRB emission, origin of which is still under debate (see Nava 2018, for review). The early emission detected in the prompt phase may have an internal origin, and

\* E-mail: ryo@phys.aoyama.ac.jp (RY)

comes from leptonic inverse-Compton process with various seed photons (Bošnjak, Daigne & Dubus 2009; Zhang, et al. 2011; Toma, Wu & Mészáros 2011; Asano & Mészáros 2012; Daigne 2012; Oganessian, et al. 2017) or from hadronic process (Asano, Inoue & Mészáros 2009; Asano & Mészáros 2012; Razzaque, Dermer & Finke 2010). The temporally extended emission is likely the afterglow synchrotron emission arising in the external shock (Kumar & Barniol Duran 2009, 2010; Ghisellini, et al. 2010; Nava, et al. 2014). Recently, Imaging Atmospheric Cherenkov Telescopes (IACTs), the Major Atmospheric Gamma Imaging Cherenkov (MAGIC) telescopes and the High Energy Stereoscopic System (H.E.S.S.), detected very-high-energy (VHE) gamma-rays from GRB 180720B (Abdalla, et al. 2019), GRB 190114C (MAGIC Collaboration, et al. 2019a) and GRB 190829A (de Naurois 2019). The VHE gamma-rays are most likely synchrotron self-Compton emission (Wang, et al. 2019; Derishev & Piran 2019; Fraija et al. 2019; MAGIC Collaboration, et al. 2019b). It is expected that in near future the number of such *VHE events* rapidly increases when Cherenkov Telescope Array (CTA; Acharya, et al. 2013) starts observations of GRBs (Kakuwa, et al. 2012; Inoue, et al. 2013; Gilmore, et al. 2013). VHE gamma-ray observations with CTA may even provide a clue to the origin of shallow decay phase in the X-ray afterglow (e.g., Murase, et al. 2010, 2011).

At present, a link between the X-ray shallow decay phase and (very-)high-energy gamma-ray emission is unclear (e.g., Panaitescu 2008). It is known that the LAT-detected GRBs are among the most energetic GRBs (Racusin, et al. 2011; Ackermann, et al. 2013; Atteia, et al. 2017; Nava, et al. 2014; Ajello et al. 2019a), so that their kinetic energy of the GRB jet may be larger than usual events without high-energy gamma-ray detection. There is also an observational implication that the initial bulk Lorentz factor of the jet is larger for LAT-detected GRBs (Ghirlanda, et al. 2012). Furthermore, emission region of the high-energy gamma-rays might have smaller magnetic-field energy density (Tak, et al. 2019). Hence one can expect that their outflow has different characteristics, so that the X-ray afterglow behaves differently. Therefore, studies of the X-ray afterglow of such extreme GRBs may provide us hints for unveiling the nature of the shallow decay phase.

In this paper, as a first step of investigating connection between the shallow decay phase and the high-energy (and VHE) gamma-ray emission, we analyze early X-ray afterglows of GRBs with detected high-energy and VHE gamma-rays. We find that their decay slopes of the shallow decay phase tend to be steeper than GRBs without high-energy/VHE gamma-ray detection, so that the X-ray shallow decay phase looks less noticeable. This fact has been already noted in previous literature very briefly (Kumar & Zhang 2015). Present work provides analysis result more quantitatively with better statistics due to larger sample size.

## 2 SAMPLE SELECTION

In this paper, we analyze early X-ray afterglows of GRBs that are detected by *Fermi*/LAT and VHE events (Sample A). For comparison, we also analyze the data of events

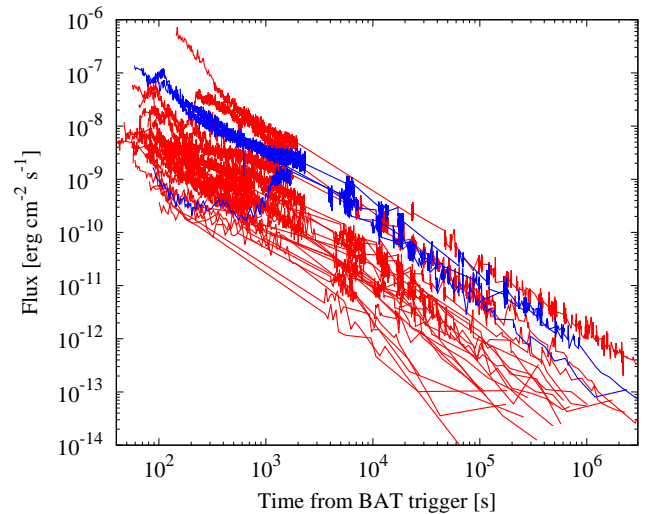


**Figure 1.** X-ray afterglow light curves of 26 events in Sample A, which consists of 23 events detected by *Fermi*/LAT but not detected by IACTs (red curves) and 3 VHE events (blue lines).

without (very-)high-energy gamma-ray emission (Samples B and C). In the following, we define our samples.

### 2.1 Sample A: GeV/TeV events

Candidate events in Sample A are taken from the second catalog of LAT-detected GRBs (Ajello et al. 2019a). The catalog includes 186 events covering from 2008 to 2018 August 4. There are 25 events in the catalog which were triggered by Burst Alert Telescope (BAT) onboard *Swift* and subsequently observed by X-ray Telescope (XRT) typically  $\sim 100$  s after the burst onset. Among them, XRT data of GRB 170813A consist of only 4 data points after the initial steep decay phase, so that we remove this event from Sample A in order to consider well-sampled early X-ray afterglow light curves. Note that a VHE event GRB 180720B is also listed in the catalog of Ajello et al. (2019a). Therefore, there are 23 events which were detected by *Fermi*/LAT but not detected by IACTs.

So far VHE gamma-rays from 3 GRBs (GRB 180720B, 190114C, and 190829A) are detected by MAGIC and H.E.S.S. (Abdalla, et al. 2019; MAGIC Collaboration, et al. 2019a; de Naurois 2019). Fortunately, all are triggered by *Swift*/BAT, so that early X-ray afterglows are observed by XRT. Hence, we include the three VHE events into Sample A, and analyze XRT data of these events. Note that two of these (GRB 180720B and 190114C) were also detected by *Fermi*/LAT, while for GRB 190829A, possible detections of sub-GeV photons have been claimed (Chand et al. 2020).

All events of Sample A are listed in Table 1, and their X-ray light curves are shown in Fig. 1. It contains 26 GRBs in total. Tang et al. (2019) and Zhao et al. (2019) collected 174 and 201 GRBs with clear shallow decay phase, respectively. Within our Sample A, only 4 events (GRB 090510, 110213A, 150403A and 180720B) overlap with the list of the former, and 3 events (GRB 090102, 090510 and 140323A) overlap with the latter. This fact already shows that there are less events hosting typical shallow decay phase in Sample A.

Finally, we note that Sample A contains a short GRB 090510. The other events are long GRBs.

## 2.2 Sample B: non-GeV events 1

We select GRBs that were triggered by *Swift*/BAT during ten years from 2008 to 2018 August 4, followed-up by XRT within 400 s after the trigger, but not detected by *Fermi*/LAT. Among them, 180 long and 3 short bursts have measured redshifts. We remove 13 events of which the number of X-ray data points after the initial steep decay phase is less than ten. We also discard 15 GRBs showing the X-ray flux rising more steeply than  $\propto t^{-1}$  as being of the different origin. Then, 155 events are remaining, and they are defined as members of Sample B and are listed in Table 2.

Although the size of Sample B is large, its members are *either* bursts that were not within the LAT field of view *or* bursts that LAT did observe the GRB field but did not detect high-energy photons. It is also noted that for Sample A the redshift measurement has not been introduced, while for Sample B it has. We believe that the latter fact does not bias our conclusion because the redshift can be determined if the event is observable with ground-based optical telescopes and this is irrelevant if the event is detected with *Swift*/BAT and/or *Fermi*/LAT. However, one might still concern that it causes some bias on the energetics/brightness of Samples A and B. Therefore, we consider another Sample C as in the next subsection.

## 2.3 Sample C: non-GeV events 2

Ackermann, et al. (2016) selected 79 GRBs, observed between 2008 August 4 and 2012 February 1, which fell in the LAT field of view at the time of trigger, but were not detected by LAT. There are 36 events in their sample whose XRT data are well, satisfying the same criteria as Samples A and B. These bursts are defined as members of Sample C, and listed in Table 3. Sample C contains no short GRBs.

The observation period during which Sample C bursts were detected was shorter than that for Sample B. There are 67 Sample B events detected in the same time period for Sample C (from GRB 080804 to 120119A), and among them only 13 GRBs are in the list of Ackermann, et al. (2016). Hence,  $13/67 \approx 19\%$  of Sample B events were in the LAT field of view at the time of trigger but they were not detected by LAT.

## 3 DATA ANALYSIS

The *Swift*/XRT data were downloaded from the *Swift* team website<sup>1</sup> (Evans et al. 2007, 2009). First the X-ray light curves in the time interval  $[t_1, t_2]$  are fitted with single power-law (SPL) function,

$$f_S(t) = f_0 t^{-\alpha_1}, \quad (1)$$

where  $f_0$  and  $\alpha_1$  are a normalization constant and a decay slope, respectively. We choose the time interval  $[t_1, t_2]$  excluding the steep decay phase and X-ray flares if they exist.

Subsequently, we also fit the light curves with double power-law (DPL) function,

$$f_D(t) = f_0 [(t/t_b)^{w\alpha_1} + (t/t_b)^{w\alpha_2}]^{-1/w}, \quad (2)$$

with  $\alpha_1$  and  $\alpha_2$  describing the decay slopes of pre- and post-break segments, respectively, and  $t_b$  is a break time. A smoothness parameter  $w$  is fixed to be 3 (Liang, Zhang & Zhang 2007; Zhao et al. 2019).

We compare above two models in order to determine whether the additional degrees of freedom in the DPL model are warranted over a simpler SPL model. We fit all light curves of our events with both models and obtain  $\chi^2$  of the best-fitting parameter set. Then, the difference between  $\chi^2$  of the two models,  $\Delta\chi^2$ , is calculated. Since there are two additional free parameters between the two models, a value of  $\Delta\chi^2 > 10$  would represent a  $> 3\sigma$  improvement in the fit. We adopt this criterion as the threshold for a statistical preference for a break in the light curve.

## 4 RESULTS

The results of the analysis on 26 events in Sample A are shown in Table 1. The upper most 5 events in the table are fitted with both SPL and DPL models, however, we find  $\Delta\chi^2 < 1$ , so that additional two parameters of the DPL model do not improve the fit. We call them *SPL events*. The other events in the table except for the lowest three VHE events have  $\Delta\chi^2 > 10$ , so that the DPL model is statistically preferred at  $> 3\sigma$  over SPL model. Hence, they are named as *DPL events* in this paper. We also analyze 3 VHE events in a similar manner, and find that two events (GRB 190114C and 190829A) are fitted with the SPL model and that the other one (GRB 180720B) is described by the DPL model. The average value of  $\alpha_1$  for 18 DPL events is  $\langle\alpha_1\rangle = 0.76$  with the standard deviation  $\sigma_{\alpha_1} = 0.40$ . When 5 SPL events are incorporated, the average value and the standard deviation become  $\langle\alpha_1\rangle = 0.89$  and  $\sigma_{\alpha_1} = 0.43$ , respectively. Further addition of 3 VHE events makes  $\langle\alpha_1\rangle = 0.92$  and  $\sigma_{\alpha_1} = 0.42$ .

Similarly, the results for Sample B are shown in Table 2. Again we define SPL and DPL events as those having  $\Delta\chi^2 < 10$  and  $> 10$ , respectively. It is found that 41 out of 155 events (26 %) are fitted with SPL. The average value of  $\alpha_1$  for 114 DPL events is  $\langle\alpha_1\rangle = 0.37$  and their standard deviation is  $\sigma_{\alpha_1} = 0.43$ . When 41 SPL events are incorporated, the average value becomes  $\langle\alpha_1\rangle = 0.54$  with the standard deviation  $\sigma_{\alpha_1} = 0.51$ . We also show the results for Sample C in Table 3. Among 36 events, only 5 events ( $5/36 \approx 14\%$ ) are explained by SPL model. The average value of  $\alpha_1$  for 31 DPL events is  $\langle\alpha_1\rangle = 0.28$  with  $\sigma_{\alpha_1} = 0.34$ . Incorporating the 5 SPL events, we get  $\langle\alpha_1\rangle = 0.40$  and  $\sigma_{\alpha_1} = 0.42$ .

Histogram in Figure 2(a) shows the distribution of  $\alpha_1$  for 5 SPL and 18 DPL events in Sample A. For the DPL events we take the best-fitting values of  $\alpha_1$  of the DPL model rather than the SPL model. Thick-dashed line represents that of Sample B. We find that 14 out of 26 events of Sample A have  $\alpha_1 > 1.05$ , that is, they depart from more than  $1\sigma$  of the whole events of Sample B. The other two Gaussian distributions (thin-dot-dashed and thin-dotted lines) are taken from Tang et al. (2019) and Zhao et al. (2019), describing the distribution of the temporal index of the typical shallow

<sup>1</sup> [https://www.swift.ac.uk/xrt\\_curves/](https://www.swift.ac.uk/xrt_curves/)

**Table 1.** Best-fitting model parameters of GRBs in Sample A.

GRB	$t_1$ – $t_2$ [ks]	SPL model : $f_S(t)$		DPL model: $f_D(t)$			$\Delta\chi^2$ <sup>a</sup>	
		$\alpha_1$	$\chi^2/\text{dof}$	$\alpha_1$	$\alpha_2$	$t_b$ [ks]		$\chi^2/\text{dof}$
Single power-law (SPL) events								
081203A	0.1–30	$1.31 \pm 0.02$	1590/297				$< 1$	
110625A	0.1–20	$1.14 \pm 0.03$	90/53				$< 1$	
121011A	0.08–12	$1.48 \pm 0.03$	38/19				$< 1$	
151006A	0.1–100	$1.40 \pm 0.01$	159/157				$< 1$	
170405A	0.2–10	$1.40 \pm 0.03$	818/206				$< 1$	
Double power-law (DPL) events								
090102	0.3–45	$1.29 \pm 0.01$	143/121	$0.21 \pm 0.36$	$1.37 \pm 0.03$	$0.62 \pm 0.11$	111/119	32
090510 <sup>c</sup>	0.07–20	$1.07 \pm 0.05$	460/70	$0.64 \pm 0.05$	$2.11 \pm 0.12$	$1.46 \pm 0.23$	103/68	357
100728A	0.8–1000	$1.26 \pm 0.01$	621/295	$1.14 \pm 0.04$	$1.65 \pm 0.06$	$16.5 \pm 6.88$	499/293	122
110213A	0.15–1000	$1.23 \pm 0.03$	2069/232	$0.04 \pm 0.06$	$1.82 \pm 0.03$	$3.26 \pm 0.17$	400/230	1669
110731A	0.09–100	$1.16 \pm 0.01$	346/268	$1.13 \pm 0.02$	$1.72 \pm 0.22$	$25.1 \pm 8.37$	332/266	15
120729A <sup>b</sup>	0.05–40	$1.18 \pm 0.02$	329/113	$1.11 \pm 0.02$	$2.82 \pm 0.38$	$8.03 \pm 1.38$	202/111	128
130427A	0.35–1000	$1.277 \pm 0.003$	2374/1409	$1.18 \pm 0.06$	$1.34 \pm 0.04$	$3.97 \pm 10.9$	2335/1407	39
130907A	0.22–100	$1.456 \pm 0.004$	4125/2296	$1.36 \pm 0.03$	$1.60 \pm 0.05$	$5.80 \pm 6.33$	3937/2294	189
140102A	0.04–10	$1.15 \pm 0.01$	804/524	$1.05 \pm 0.02$	$1.55 \pm 0.07$	$1.71 \pm 0.51$	668/522	137
140323A	0.2–100	$0.82 \pm 0.02$	551/112	$0.60 \pm 0.03$	$1.67 \pm 0.10$	$10.2 \pm 1.76$	184/110	367
150314A	0.09–110	$1.08 \pm 0.01$	1532/674	$0.90 \pm 0.01$	$1.47 \pm 0.03$	$2.32 \pm 0.36$	951/672	581
150403A	0.2–100	$1.04 \pm 0.01$	6385/1601	$0.43 \pm 0.02$	$1.27 \pm 0.01$	$1.28 \pm 0.07$	1813/1599	4572
160325A	0.2–10	$1.36 \pm 0.02$	202/128	$0.98 \pm 0.29$	$1.53 \pm 0.11$	$0.45 \pm 0.47$	182/126	20
160905A	0.1–100	$0.96 \pm 0.01$	3796/989	$0.66 \pm 0.02$	$1.35 \pm 0.02$	$1.48 \pm 0.14$	1495/987	2301
160917A <sup>b</sup>	0.07–25	$1.25 \pm 0.02$	52.4/32	$1.22 \pm 0.03$	$2.33 \pm 0.72$	$12.2 \pm 4.25$	42.2/30	10.2
170728B	0.3–20	$0.99 \pm 0.01$	374/196	$0.32 \pm 0.17$	$1.22 \pm 0.03$	$1.21 \pm 0.32$	275/194	99
170906A	0.2–30	$1.26 \pm 0.03$	2055/267	$0.35 \pm 0.05$	$1.91 \pm 0.14$	$1.14 \pm 0.30$	450/265	1605
171120A	3–150	$0.61 \pm 0.04$	173/75	$0.39 \pm 0.06$	$1.77 \pm 0.24$	$37.0 \pm 8.2$	87/73	85
Very-high-energy gamma-ray (VHE) events								
180720B	0.25–100	$0.931 \pm 0.004$	7233/3361	$0.74 \pm 0.01$	$1.43 \pm 0.02$	$4.70 \pm 0.23$	4731/3359	2502
190114C	0.065–100	$1.338 \pm 0.004$	1822/1030					$< 1$
190829A	2–100	$1.33 \pm 0.02$	451/235					$< 1$

**Notes.**<sup>a</sup> A DPL model is statistically preferred at  $> 3\sigma$  over a simpler SPL model when  $\Delta\chi^2 > 10$ .<sup>b</sup> Best-fitting values of  $\alpha_1$  and  $\alpha_2$  of DPL model are consistent with the jet break (see section 5).<sup>c</sup> A short GRB.

decay phase. It is found that events in Sample A (including VHE events shown by arrows) tend to have larger value of  $\alpha_1$  than those with typical shallow decay phase. It is also noted that the SPL events sit the upper end of the  $\alpha_1$  distribution. If  $\alpha_1 > 1$ , the decay phase is no longer the shallow decay phase, but the normal decay phase. The same plot but for Sample C is shown in Figure 2(b). It is indicated that Sample C events have smaller value of  $\alpha_1$  than those of Samples A and B.

To see the decay properties of the DPL events in more detail, we show in Figure 3 the best-fitting parameters ( $\alpha_1$ ,  $\alpha_2$  and  $t_b$ ) of DPL events of Samples A (red squares) in the  $\alpha_1-t_b$  (left panel) and  $\alpha_1-\alpha_2$  planes (right panel). Smaller grey dots are those of Sample B, while larger green dots are of Sample C. It is found from Fig. 3 that compared with events of Sample B, roughly a half of 18 Sample A DPL events as well as a VHE event (GRB 180720B) have larger pre-break decay index  $\alpha_1$  while the break time  $t_b$  and the post-break decay index  $\alpha_2$  are roughly similar. Figure 4 supports this claim. More quantitatively, 15 out of 18 Sample A DPL events as well as the VHE event GRB 180720B have values of  $\alpha_2$  within  $1\sigma$  range of Sample B (dashed line in the right panel of Figure 4), and 13 out of the 19 Sample A events have values of  $t_b$  within  $1\sigma$  range of Sample B (dashed line in the left panel of Figure 4). According to these results,

we schematically draw in Figure 5 the typical behavior of GRBs in Sample A.

**5 DISCUSSION**

In the  $\alpha_1-\alpha_2$  plane for DPL events, there are two data points from Sample A (GRB 120729 and 160917A) whose best-fitting values  $\alpha_1 > 1$  and  $\alpha_2 > 2$ . Although the break time  $t_b \sim 10^4$  s for these bursts, the measured break should be taken as a jet break rather than the *shallow-to-normal* break. According to the theory of the jet break, if the X-ray afterglow is in the slow cooling regime with the X-ray band frequency larger than the cooling frequency  $\nu_c$ , then the decay indices are given by  $(3p-2)/4$  and  $p$  for pre- and post-jet break, respectively, where  $p$  is an index of the power-law electron distribution (Sari, Piran & Halpern 1999). For GRB 160917A, if the measured value of  $\alpha_1 = 1.22 \pm 0.03$  corresponds to the pre-jet break decay index, then we have  $p = (2 + 4\alpha_1)/3 = 2.29 \pm 0.04$ , so that the observed value of  $\alpha_2 = 2.33 \pm 0.72$  is consistent with the post-jet break decay index within  $1\sigma$  error. On the other hand, GRB 120729A may not follow the jet break theory. Similar calculation for GRB 120729A leads to  $p = (2 + 4\alpha_1)/3 = 2.15 \pm 0.03$ , which is somewhat smaller than the measured post-break index  $\alpha_2 = 2.82 \pm 0.38$  but still consistent within  $2\sigma$  er-

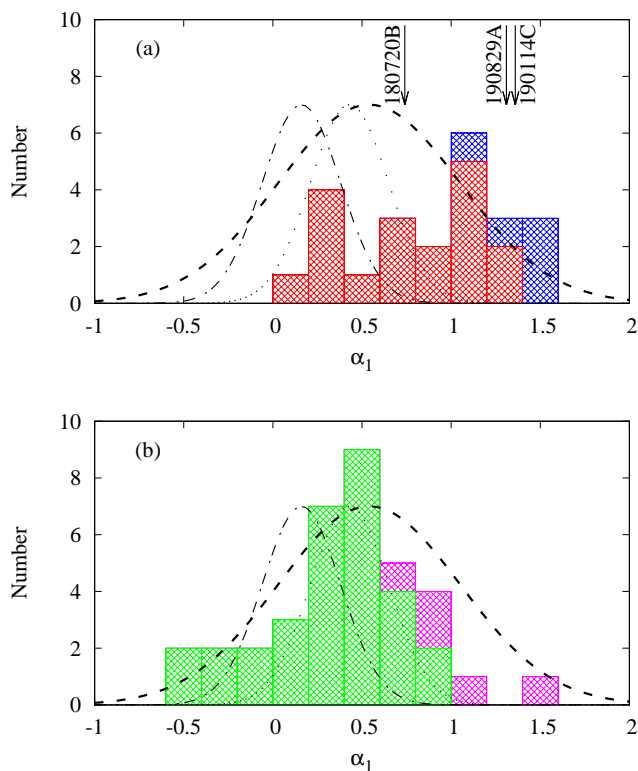


**Figure 2.** (a) Blue and red histograms show the distributions of the decay slope  $\alpha_1$  for 5 SPL and 18 DPL events, respectively, in Sample A. Thick-dashed line represents the same distribution for the whole Sample B events (155 events;  $\langle\alpha_1\rangle = 0.54$  and  $\sigma_{\alpha_1} = 0.51$ ). Thin-dot-dashed and thin dotted lines are those for long GRBs with typical shallow decay phase taken from Tang et al. (2019) and Zhao et al. (2019), respectively. Also shown are arrows describing the values of  $\alpha_1$  for 3 VHE events. (b) Magenta and green histograms show the  $\alpha_1$  distribution of 5 SPL and 31 DPL events, respectively, in Sample C. The three lines are the same as those in panel (a).

ror. Nevertheless, the post-break decay index  $\alpha_2$  is too steep for the normal decay phase of the X-ray afterglow. Therefore, these bursts should be treated as events without shallow decay phase. Also in Sample B, there are two events (GRB 110818A and 120119A) having  $\alpha_1 > 1$  and  $\alpha_2 > 2$ . They are also regarded as bursts without shallow decay phase.

Taking into account the correction described in the previous paragraph, we calculate for Sample A the fraction of events without shallow decay phase as 5 SPL as well as 2 DPL events (GRB 120729 and 160917A) out of 23 events, so that  $7/23 \approx 30\%$ . In order to compare this fraction with that of Sample B, we need more careful treatment of 41 bursts in Sample B being claimed as SPL events. Among them, there are 18 events which show only X-ray flares until 3 ks after the burst trigger, possibly overlying shallow and normal decay phases. In addition, there are 4 bursts showing longer initial steep decay phase until 2 ks without steep-to-shallow break. These 22 events should be excluded, and we regard the remaining 19 events as bursts without clear shallow decay phase. Hence, the fraction of events without shallow decay phase as these 19 events as well as 2 DPL

events described in the previous paragraph (GRB 110818A and 120119A) out of 155 events, so that  $21/155 \approx 14\%$ . The same argument can be done for Sample C. Among 5 SPL events, there are 3 bursts showing only X-ray flares until 3 ks, and there is an event with long initial steep decay phase lasting 2 ks (see Table 3). Then, we get the fraction of events without shallow decay phase as  $1/36 \approx 3\%$ . Although sample selection method is different from ours, Liang, et al. (2009) reported the number,  $19/400 \approx 5\%$ , for all long GRBs with XRT detection from 2005 January to 2009 July.

Furthermore, two (GRB 190114C and 190829A) out of 3 VHE events detected so far have no shallow decay phase. Even if X-ray light curve has a break, 12 events out of 18 in Sample A have the pre-break decay index  $\alpha_1$  larger than the mean value,  $\langle\alpha_1\rangle = 0.37$ , of DPL events in Sample B. In addition, Zhao et al. (2019) derived a mean of  $\langle\alpha_1\rangle = 0.43$  and a dispersion of 0.22 (see thin-dotted line in Fig. 2) for events showing typical shallow decay phase. If we take into account their result, 8 DPL events in our Sample A have  $\alpha_1 > 0.7$ , deviating from the mean of Zhao et al. (2019) more than  $1\sigma$ . Hence one can say that a large fraction (17 out of 26 events) of GRBs detected in high-energy and VHE gamma-ray bands has no shallow decay phase, or they have less noticeable shallow decay phase in the early X-ray afterglow.

It would be interesting to investigate whether the difference in the X-ray behavior seen in this study is found between more and less energetic/powerful GRBs or rather between GRBs with (very-)high-energy gamma-ray emission and GRBs not producing the high-energy radiation. In order to approach this issue, we plot in Figure 6 the distribution of isotropic equivalent gamma-ray energy in 15–150 keV,  $E_{\text{iso}}$ , of GRBs with measured redshift. A Kolmogorov-Smirnov (KS) tests on the two distributions from different samples are performed. For  $E_{\text{iso}}$  distributions of Sample A and Sample B (Sample C), we get 0.33 % (1.1 %) probability of being drawn from a common population. Hence, it is indicated that Sample A bursts tend to have larger  $E_{\text{iso}}$ . Another KS test on the  $E_{\text{iso}}$  distributions of Samples B and C gave the probability of 79 %, so that we find no difference between Samples B and C with respect to the burst energy. Therefore, differences between GeV/TeV events (Sample A) and general samples (Samples B and C) might be a result of the difference between more and less energetic GRBs.

Our present result may constrain models of the shallow decay phase of the X-ray afterglow. In the context of the energy injection model (Nousek, et al. 2006; Zhang, et al. 2006; Granot & Kumar 2006; Kobayashi & Zhang 2007), initial outflow energy is small, so that the X-ray afterglow arising from the external shock is initially dim. If the additional energy is injected to the flow, then the X-ray afterglow becomes brighter than that in the case of no energy injection, resulting in the shallow decay phase. As seen in the previous paragraph, high-energy gamma-ray events tend to have larger isotropic gamma-ray energy of the prompt emission (see also Ackermann, et al. 2013; Atteia, et al. 2017; Nava, et al. 2014; Ajello et al. 2019a), hence it is expected that the initial outflow energy is also large. In this case, the X-ray afterglow is already bright from the beginning, and it shows no shallow decay phase. Therefore, this model naturally explains the present result that a large fraction of events of our sample have no clear shallow decay phase.

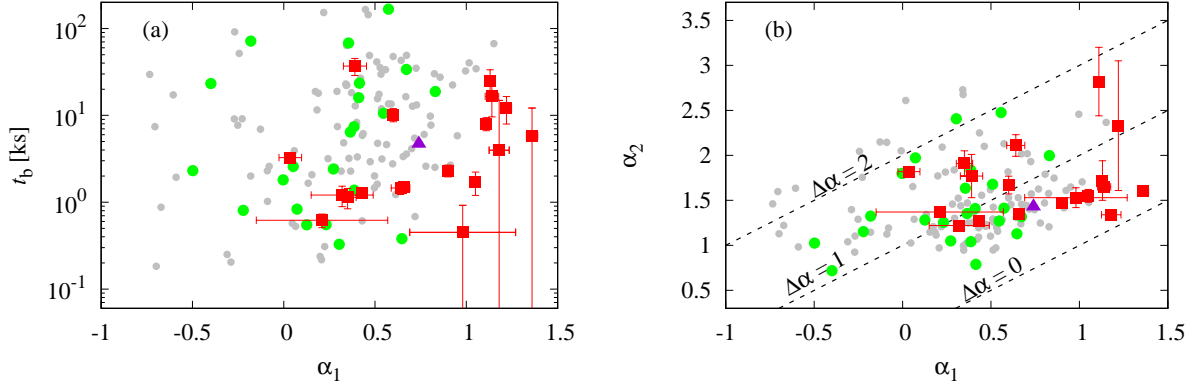


**Figure 3.** Comparison of 18 DPL events (red squares) of Sample A and a VHE event (GRB 180720B: violet triangle) to bursts of Sample B (smaller grey dots) and Sample C (larger green dots) in  $\alpha_1$ – $t_b$  plane (left panel) and  $\alpha_1$ – $\alpha_2$  plane (right panel).

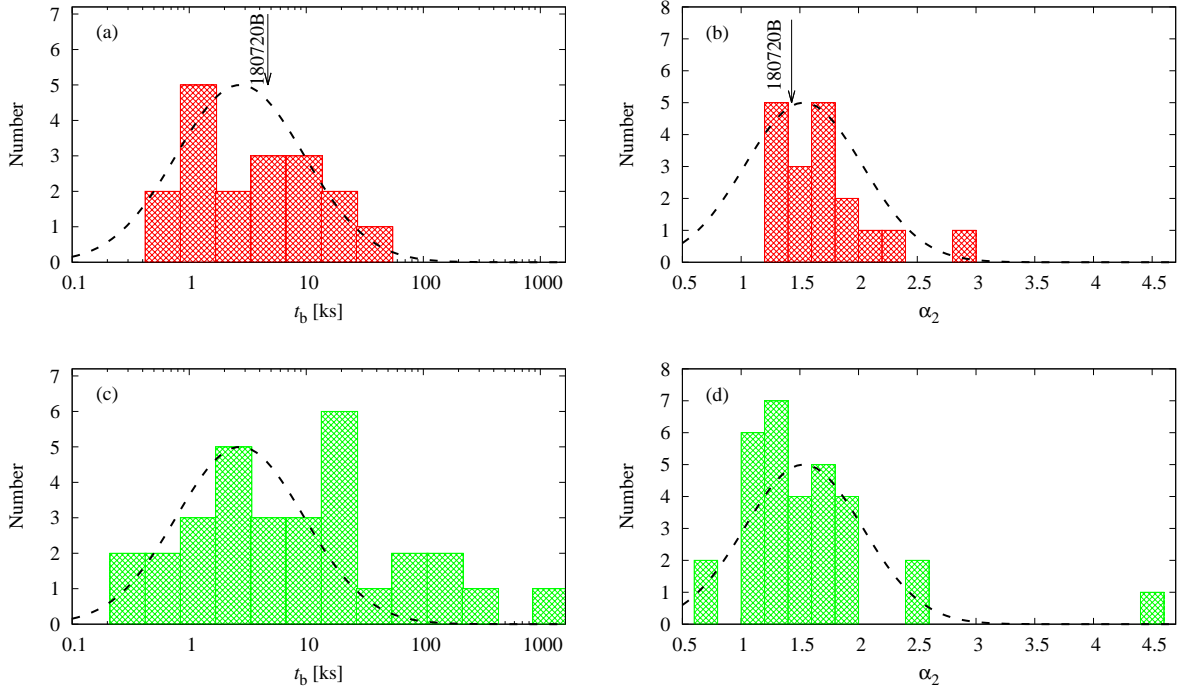


**Figure 4.** Red histograms in panels (a) and (b) show the distributions of the break time  $t_b$  and the post-break decay index  $\alpha_2$  of 18 DPL events in Sample A, respectively. Panels (c) and (d) are the same as (a) and (b), respectively, but for Sample C. Thick-dashed lines are for 114 DPL events in Sample B. For Sample B, the mean and the standard deviation of  $t_b$  are  $\langle \log_{10}(t_b/\text{ks}) \rangle = 0.44$  and  $\sigma_{t_b} = 0.54$  dex, respectively [panels (a) and (c)], and the mean and the standard deviation of  $\alpha_2$  are  $\langle \alpha_2 \rangle = 1.53$  and  $\sigma_{\alpha_2} = 0.50$ , respectively [panels (b) and (d)]. Also shown in panels (a) and (b) are arrows describing the values of a VHE event, GRB 180720B.

Some other models will be challenged if more data are accumulated in future.

We also search for any correlation between X-ray light curve parameters like  $\alpha_1$  and  $t_b$  and GeV properties listed in the second catalog of LAT-detected GRBs (Ajello et al. 2019a), such as the temporal decay index  $\alpha_{\text{GeV}}$ , spectral index  $\beta$ , and isotropic energy of the gamma-ray emission in the LAT energy band  $E_{\text{iso}}$ . Among  $2 (\alpha_1 \text{ and } t_b) \times 3 (\alpha_{\text{GeV}}, \beta \text{ and } E_{\text{iso}}) = 6$  combinations, we find no statistically significant correlation because of small sample size.

More events are necessary to have larger sample, and further analysis with better statistics is left for future work.

## ACKNOWLEDGMENTS

We would like to thank Drs. K. Asano, K. Ioka, Y. Ohira and S. J. Tanaka for valuable comments to improve this paper. This work made use of data supplied by the UK Swift Science Data Centre at the University of Leicester. We also thank the referee for his or her thoughtful comments to improve the paper. This work is supported in

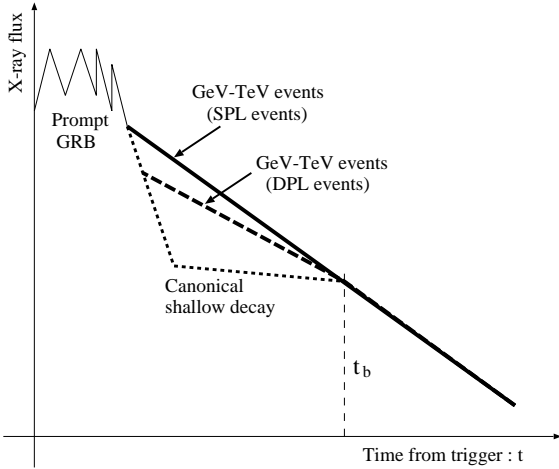


**Figure 5.** Schematic view of early X-ray afterglow light curves of 26 events considered in this paper. Nine events (5 SPL and 2 DPL events as well as 2 VHE events) have no shallow decay phase. Eight events (7 DPL events and a VHE event) have a break but their pre-break index  $\alpha_1 > 0.7$ , so that the decay slope before the break time  $t_b$  is somewhat steeper than typical shallow decay phase.

part by grant-in-aid from the Ministry of Education, Culture, Sports, Science, and Technology (MEXT) of Japan, No.18H01232(RY), No.17H06362(TS), No.18H01257(TS), and No.17K05402(MS). R.Y. and T.S. deeply appreciate Aoyama Gakuin University Research Institute for helping our research by the fund.

*Facilities: Swift and Fermi.*

## REFERENCES

- Abdalla H., et al., 2019, *Nature*, 575, 464  
 Acharya B. S., et al., 2013, *APh*, 43, 3  
 Ackermann M., et al., 2013, *ApJS*, 209, 11  
 Ackermann M., et al., 2016, *ApJ*, 822, 68  
 Ajello M., et al., 2019a, *ApJ*, 878, 52  
 Asano K., Inoue S., Mészáros P., 2009, *ApJ*, 699, 953  
 Asano K., Mészáros P., 2012, *ApJ*, 757, 115  
 Atteia J.-L., et al., 2017, *ApJ*, 837, 119  
 Beniamini P., Duque R., Daigne F., Mochkovitch R., 2020, *MNRAS*, 492, 2847  
 Bošnjak Ž., Daigne F., Dubus G., 2009, *A&A*, 498, 677  
 Chand V. et al. 2020, preprint (arXiv:2001.00648)  
 Dado S., Dar A., De Rújula A., 2006, *ApJL*, 646, L21  
 Daigne F., 2012, *IJMPS*, 8, 196  
 Dainotti M. G., Willingale R., Capozziello S., Fabrizio Cardone V., Ostrowski M., 2010, *ApJL*, 722, L215  
 Dainotti M. G., Petrosian V., Singal J., Ostrowski M., 2013, *ApJ*, 774, 157  
 Dainotti M. G., Postnikov S., Hernandez X., Ostrowski M., 2016, *ApJL*, 825, L20  
 de Naurois M. (H. E. S. S. Collaboration), 2019, *The Astronomer's Telegram*, 13052  
 Derishev E., Piran T., 2019, *ApJL*, 880, L27  
 Eichler D., Granot J., 2006, *ApJL*, 641, L5  
 Evans P. A., Beardmore A. P., Page K. L., et al. 2007, *A&A*, 469, 379

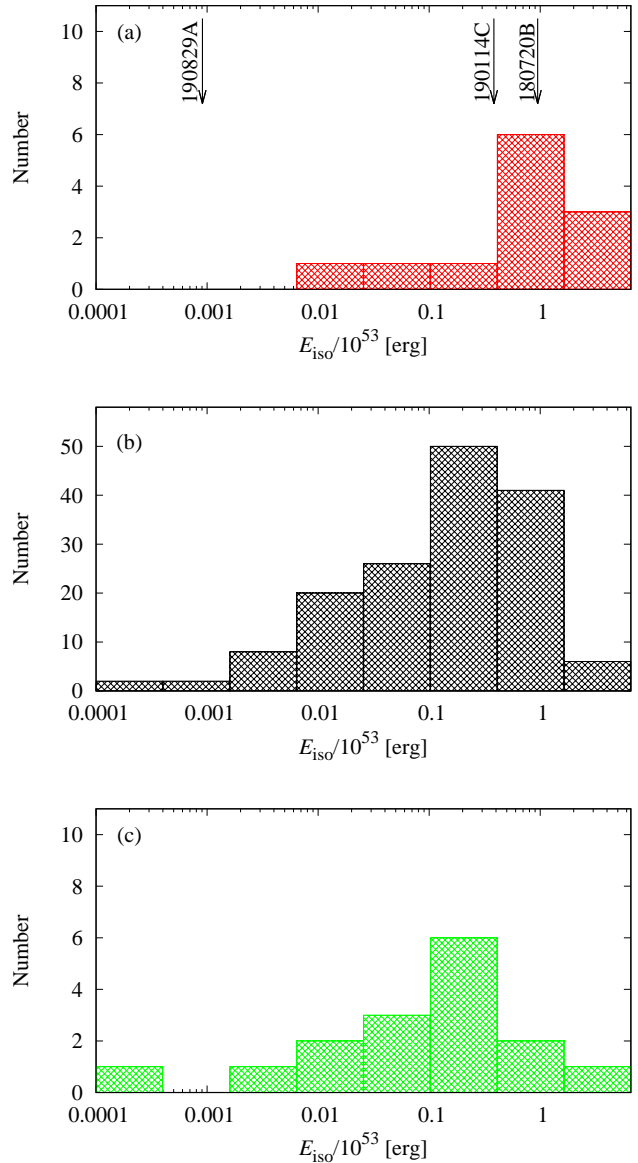


**Figure 6.** The distributions of isotropic gamma-ray energy of the prompt emission,  $E_{\text{iso}}$ , for events with measured redshift in Sample A [panel (a)], Sample B [panel (b)] and Sample C [panel (c)]. Arrows in panel (a) describe the values of three VHE events.

- Evans P. A., Beardmore A. P., Page K. L., et al. 2009, *MNRAS*, 397, 1177  
 Fan Y., Piran T., 2006, *MNRAS*, 369, 197  
 Fraija N., Barniol Duran R., Dichiara S., Beniamini P., 2019, *ApJ*, 883, 162  
 Genet F., Daigne F., Mochkovitch R., 2007, *MNRAS*, 381, 732  
 Ghirlanda G., Nava L., Ghisellini G., Celotti A., Burlon D., Covino S., Melandri A., 2012, *MNRAS*, 420, 483  
 Ghisellini G., Ghirlanda G., Nava L., Celotti A., 2010, *MNRAS*, 403, 926  
 Ghisellini G., Ghirlanda G., Nava L., Firmani C., 2007, *ApJL*, 658, L75  
 Gilmore R. C., Bouvier A., Connaughton V., Goldstein A., Otte N., Primack J. R., Williams D. A., 2013, *ExA*, 35,

413

- Granot J., Königl A., Piran T., 2006, MNRAS, 370, 1946  
 Granot J., Kumar P., 2006, MNRAS, 366, L13  
 Inoue S., et al., 2013, APh, 43, 252  
 Ioka K., Toma K., Yamazaki R., Nakamura T., 2006, A&A, 458, 7  
 Kakuwa J., Murase K., Toma K., Inoue S., Yamazaki R., Ioka K., 2012, MNRAS, 425, 514  
 Kobayashi S., Zhang B., 2007, ApJ, 655, 973  
 Kumar P., Barniol Duran R., 2009, MNRAS, 400, L75  
 Kumar P., Barniol Duran R., 2010, MNRAS, 409, 226  
 Kumar P., Panaitescu A., 2000, ApJL, 541, L51  
 Kumar P., Zhang B., 2015, PhR, 561, 1  
 Liang E.-W., Zhang B.-B., Zhang B., 2007, ApJ, 670, 565  
 Liang E.-W., Racusin J. L., Zhang B., Zhang B.-B., Burrows D. N., 2008, ApJ, 675, 528  
 Liang E.-W., Lü H.-J., Hou S.-J., Zhang B.-B., Zhang B., 2009, ApJ, 707, 328  
 MAGIC Collaboration, et al., 2019a, Nature, 575, 455  
 MAGIC Collaboration, et al., 2019b, Nature, 575, 459  
 Margutti R., et al., 2013, MNRAS, 428, 729  
 Murase K., Toma K., Yamazaki R., Nagataki S., Ioka K., 2010, MNRAS, 402, L54  
 Murase K., Toma K., Yamazaki R., Mészáros P., 2011, ApJ, 732, 77  
 Nava L., et al., 2014, MNRAS, 443, 3578  
 Nava L., 2018, IJMPD, 27, 1842003  
 Nousek J. A., et al., 2006, ApJ, 642, 389  
 Oganessian G., Nava L., Ghirlanda G., Celotti A., 2017, ApJ, 846, 137  
 Oganessian G., Ascenzi S., Branchesi M., Sharan Salafia O., Dall’Osso S., Ghirlanda G., 2019, arXiv:1904.08786  
 Panaitescu A., 2008, MNRAS, 385, 1628  
 Racusin J. L., et al., 2009, ApJ, 698, 43  
 Racusin J. L., et al., 2011, ApJ, 738, 138  
 Razzaque S., Dermer C. D., Finke J. D., 2010, OAJ, 3, 150  
 Sakamoto T., et al., 2008, ApJ, 679, 570  
 Sari R., Piran T., Narayan R., 1998, ApJL, 497, L17  
 Sari R., Piran T., Halpern J. P., 1999, ApJL, 519, L17  
 Sultana J., Kazanas D., Mastichiadis A., 2013, ApJ, 779, 16  
 Tak D., Omodei N., Uhm Z. L., Racusin J., Asano K., McEnery J., 2019, ApJ, 883, 134  
 Tang C.-H. et al. 2019, Tang C.-H., Huang Y.-F., Geng J.-J., Zhang Z.-B., 2019, ApJS, 245, 1  
 Toma K., Ioka K., Yamazaki R., Nakamura T., 2006, ApJL, 640, L139  
 Toma K., Wu X.-F., Mészáros P., 2011, MNRAS, 415, 1663  
 van Eerten H. J., 2014, MNRAS, 445, 2414  
 Wang X.-Y., Liu R.-Y., Zhang H.-M., Xi S.-Q., Zhang B., 2019, ApJ, 884, 117  
 Willingale R., et al., 2007, ApJ, 662, 1093  
 Yamazaki R., Toma K., Ioka K., Nakamura T., 2006, MNRAS, 369, 311  
 Yamazaki R., 2009, ApJL, 690, L118  
 Zhang B., et al., 2006, ApJ, 642, 354  
 Zhang B.-B., et al., 2011, ApJ, 730, 141  
 Zhao L. et al. 2019, ApJ, 883, 97

**Table 2.** Best-fitting model parameters of GRBs in Sample B.

GRB	$t_1-t_2$ [ks]	SPL model : $f_S(t)$		DPL model: $f_D(t)$				$\Delta\chi^2$ <sup>a</sup>
		$\alpha_1$	$\chi^2/dof$	$\alpha_1$	$\alpha_2$	$t_b$ [ks]	$\chi^2/dof$	
Single power-law (SPL) events								
080804	0.1–1000	$1.09 \pm 0.01$	105/101	$1.02 \pm 0.25$	$1.15 \pm 0.16$	$1.0 \pm 16.8$	104/99	1
080805 <sup>d</sup>	3–1000	$0.94 \pm 0.03$	27/22	$-0.08 \pm 3.14$	$0.97 \pm 0.06$	$4.55 \pm 1.87$	26/20	1
080916A	0.2–1000	$0.98 \pm 0.02$	170/69					< 1
081118 <sup>e</sup>	0.9–1000	$0.60 \pm 0.05$	13/8	$0.49 \pm 0.25$	$0.77 \pm 0.75$	$138 \pm 1210$	11/6	2
081210 <sup>d</sup>	5–200	$0.67 \pm 0.03$	18/21					< 1
090417B <sup>d</sup>	5–1000	$1.38 \pm 0.02$	126/118					< 1
090423 <sup>d</sup>	3–500	$1.37 \pm 0.04$	39/38	$1.13 \pm 0.31$	$1.60 \pm 0.24$	$17.6 \pm 40.8$	34/36	5
090715B <sup>d</sup>	0.45–2000	$1.18 \pm 0.02$	149/74	$1.09 \pm 0.29$	$1.25 \pm 0.19$	$5.5 \pm 75.7$	145/72	4
090812	0.4–200	$1.23 \pm 0.02$	227/92					< 1
090814A	0.1–200	$2.05 \pm 0.04$	623/113					< 1
090926B	0.5–10	$1.17 \pm 0.06$	30/25					< 1
100513A	0.5–1000	$0.89 \pm 0.04$	91/28					< 1
101213A <sup>e</sup>	0.5–1000	$0.91 \pm 0.02$	102/71	$0.43 \pm 1.22$	$0.94 \pm 0.05$	$0.65 \pm 0.72$	98/69	4
110205A	0.8–300	$1.63 \pm 0.01$	188/145					< 1
110801A <sup>d</sup>	0.55–100	$1.41 \pm 0.02$	411/111					< 1
111107A <sup>d</sup>	0.7–100	$0.83 \pm 0.04$	15/13	$0.10 \pm 0.79$	$0.93 \pm 0.09$	$1.32 \pm 0.91$	12/11	3
111225A <sup>d</sup>	0.7–100	$1.40 \pm 0.08$	46/10					< 1
120712A	0.8–500	$1.20 \pm 0.04$	86/33	$-0.56 \pm 2.20$	$1.25 \pm 0.06$	$1.06 \pm 0.26$	80/31	6
121201A	0.1–100	$1.25 \pm 0.03$	74/33					< 1
121211A <sup>d</sup>	3–400	$0.91 \pm 0.04$	128/68					< 1
130131B <sup>d</sup>	0.2–20	$1.00 \pm 0.07$	16/9	$0.02 \pm 0.70$	$1.25 \pm 0.27$	$0.64 \pm 0.54$	10/7	6
130427B	0.2–100	$1.07 \pm 0.04$	34/19					< 1
130610A	1–300	$1.19 \pm 0.03$	20/26	$-0.20 \pm 2.67$	$1.23 \pm 0.06$	$1.36 \pm 0.46$	19/24	1
130701A	0.07–70	$1.16 \pm 0.01$	250/128	$1.12 \pm 0.05$	$1.41 \pm 0.30$	$17.9 \pm 39.7$	242/126	8
131103A <sup>d</sup>	1–100	$1.13 \pm 0.04$	60/36					< 1
140304A <sup>d</sup>	1–300	$1.31 \pm 0.12$	478/24					< 1
140515A <sup>d</sup>	6–300	$1.20 \pm 0.06$	88/38					< 1
140907A <sup>d</sup>	3–1000	$0.98 \pm 0.03$	88/57	$0.78 \pm 0.98$	$1.07 \pm 0.39$	$7.2 \pm 71.6$	87/55	1
141109A	0.1–3000	$1.40 \pm 0.01$	3693/497					< 1
141221A <sup>d</sup>	3–200	$1.17 \pm 0.05$	21/16					< 1
150301B	0.2–80	$1.06 \pm 0.03$	16/16	$0.07 \pm 1.20$	$1.12 \pm 0.08$	$0.26 \pm 0.15$	13/14	3
150727A	2–1000	$0.81 \pm 0.09$	22/8					< 1
150818A <sup>d</sup>	4–1000	$0.73 \pm 0.03$	20/14					< 1
150821A <sup>d</sup>	5–300	$1.32 \pm 0.04$	31/30	$1.14 \pm 0.38$	$1.60 \pm 0.46$	$33.8 \pm 115$	29/28	2
160117B	1–300	$0.91 \pm 0.03$	37/29					< 1
160131A	0.05–600	$1.18 \pm 0.01$	1504/596					< 1
160203A <sup>e</sup>	4–500	$1.16 \pm 0.06$	8/12					< 1
160425A	0.5–1000	$0.95 \pm 0.02$	130/65					< 1
170604A <sup>d</sup>	2–2000	$1.09 \pm 0.02$	149/92					< 1
171222A <sup>e</sup>	1–1000	$0.61 \pm 0.04$	56/15	$0.57 \pm 0.06$	$1.56 \pm 1.91$	$540 \pm 552$	51/13	5
180205A	0.3–1000	$0.98 \pm 0.02$	72/37	$0.65 \pm 0.49$	$1.07 \pm 0.06$	$1.02 \pm 1.85$	63/35	9
Double power-law (DPL) events								
080810	0.4–1000	$1.25 \pm 0.04$	304/71	$0.77 \pm 0.05$	$1.63 \pm 0.05$	$6.02 \pm 1.24$	76/69	228
080905B	0.2–1000	$0.95 \pm 0.03$	890/85	$0.33 \pm 0.08$	$1.44 \pm 0.04$	$4.84 \pm 1.28$	152/83	738
080928	3–100	$1.51 \pm 0.06$	187/72	$0.39 \pm 0.56$	$1.84 \pm 0.11$	$7.41 \pm 1.85$	145/70	42
081007	0.7–1000	$0.87 \pm 0.03$	156/50	$0.64 \pm 0.05$	$1.31 \pm 0.10$	$43.0 \pm 18.5$	65/48	91
081008	0.5–1000	$1.06 \pm 0.04$	235/53	$0.83 \pm 0.03$	$2.00 \pm 0.10$	$18.8 \pm 3.0$	49/51	186
081221	0.3–1000	$1.21 \pm 0.01$	478/247	$0.07 \pm 0.18$	$1.29 \pm 0.02$	$0.53 \pm 0.06$	296/245	182
081222	0.1–100	$1.03 \pm 0.01$	654/368	$0.65 \pm 0.08$	$1.13 \pm 0.02$	$0.38 \pm 0.14$	492/366	162
090113	0.1–400	$1.10 \pm 0.04$	100/25	$0.13 \pm 0.22$	$1.28 \pm 0.05$	$0.55 \pm 0.16$	38 /23	62
090205	0.4–100	$0.74 \pm 0.05$	125/31	$-0.08 \pm 0.19$	$1.19 \pm 0.10$	$2.59 \pm 0.62$	50/29	75
090407	0.9–1000	$0.65 \pm 0.04$	599/111	$0.36 \pm 0.03$	$1.63 \pm 0.09$	$68.1 \pm 8.3$	181/109	418
090418A	0.2–100	$0.93 \pm 0.03$	249/87	$0.37 \pm 0.10$	$1.47 \pm 0.06$	$2.28 \pm 0.43$	94/85	155
090424	0.1–5000	$1.05 \pm 0.01$	1421/658	$0.83 \pm 0.02$	$1.21 \pm 0.01$	$2.52 \pm 0.65$	828/656	593
090426 <sup>c</sup>	0.1–600	$0.96 \pm 0.04$	54/28	$-0.31 \pm 0.54$	$1.04 \pm 0.04$	$0.25 \pm 0.06$	31/26	23
090530	0.4–1000	$0.76 \pm 0.04$	171/46	$0.51 \pm 0.04$	$1.29 \pm 0.12$	$41.2 \pm 14.5$	63/44	108
090618	0.3–3000	$1.07 \pm 0.01$	4158/1151	$0.80 \pm 0.01$	$1.47 \pm 0.01$	$9.79 \pm 0.72$	1739/1149	2419
090809	10–300	$1.22 \pm 0.13$	39/13	$-0.61 \pm 0.59$	$1.63 \pm 0.15$	$17.2 \pm 3.49$	10/11	29
091018	0.03–1000	$0.99 \pm 0.01$	656/139	$0.43 \pm 0.06$	$1.20 \pm 0.02$	$0.61 \pm 0.14$	232/137	424
091020	0.3–300	$1.07 \pm 0.01$	315/171	$1.02 \pm 0.02$	$1.71 \pm 0.13$	$40.3 \pm 9.8$	240/169	75
091029	0.6–1000	$0.73 \pm 0.03$	727/125	$0.18 \pm 0.05$	$1.15 \pm 0.03$	$11.6 \pm 1.6$	177/123	550

**Table 2** – *continued*

GRB	$t_1-t_2$ [ks]	SPL model : $f_S(t)$		DPL model: $f_D(t)$			$\Delta\chi^2$ <sup>a</sup>	
		$\alpha_1$	$\chi^2/dof$	$\alpha_1$	$\alpha_2$	$t_b$ [ks]		
091109A	0.3–1000	$0.91 \pm 0.03$	29/24	$0.36 \pm 0.43$	$1.02 \pm 0.04$	$1.13 \pm 0.82$	17/22	12
091208B	0.2–1000	$0.97 \pm 0.02$	199/59	$-0.22 \pm 0.25$	$1.15 \pm 0.03$	$0.81 \pm 0.14$	86/57	113
100219A	0.8–200	$0.73 \pm 0.07$	184/25	$0.56 \pm 0.04$	$3.74 \pm 0.35$	$33.6 \pm 2.7$	29/23	155
100302A	1–1000	$0.71 \pm 0.04$	48/23	$0.35 \pm 0.11$	$0.95 \pm 0.07$	$22.3 \pm 13.1$	18/21	30
100316B	0.1–500	$0.92 \pm 0.11$	121/13	$0.13 \pm 0.14$	$1.34 \pm 0.19$	$1.66 \pm 1.32$	18/11	103
100316D	0.1–1000	$0.63 \pm 0.04$	3950/402	$0.07 \pm 0.03$	$1.97 \pm 0.04$	$0.83 \pm 0.01$	529/400	3421
100418A	0.9–1000	$0.47 \pm 0.10$	294/21	$-0.18 \pm 0.07$	$1.33 \pm 0.11$	$71.5 \pm 14.6$	26/19	268
100424A	0.08–30	$1.33 \pm 0.04$	748/165	$0.22 \pm 0.09$	$2.09 \pm 0.06$	$0.31 \pm 0.02$	205/163	543
100425A	0.25–1000	$0.69 \pm 0.04$	64/22	$0.52 \pm 0.05$	$1.19 \pm 0.13$	$29.6 \pm 14.8$	21/20	43
100508A	0.8–200	$0.74 \pm 0.08$	516/48	$0.34 \pm 0.04$	$2.73 \pm 0.19$	$22.9 \pm 1.8$	71/46	445
100615A	0.2–200	$3.16 \pm 0.32$	52920/81	$0.32 \pm 0.03$	$1.22 \pm 0.09$	$15.8 \pm 3.5$	92/79	52828
100621A	0.4–2000	$0.95 \pm 0.02$	822/185	$0.37 \pm 0.04$	$1.25 \pm 0.10$	$18.2 \pm 4.1$	85/76	737
100724A <sup>c</sup>	0.1–400	$1.03 \pm 0.05$	60/17	$0.70 \pm 0.13$	$1.44 \pm 0.12$	$4.14 \pm 2.53$	27/15	33
100728B	0.08–100	$1.05 \pm 0.02$	68/37	$0.95 \pm 0.08$	$1.65 \pm 0.34$	$5.83 \pm 5.64$	41/35	27
100814A	0.5–1000	$0.73 \pm 0.02$	1848/320	$0.46 \pm 0.02$	$2.10 \pm 0.08$	$144 \pm 8.3$	524/318	1324
100901A	0.01–2	$0.96 \pm 0.03$	1416/233	$-0.73 \pm 0.10$	$1.46 \pm 0.03$	$29.6 \pm 1.21$	363/231	1053
100905A	0.6–100	$0.90 \pm 0.07$	32/12	$0.15 \pm 0.51$	$1.15 \pm 0.16$	$2.07 \pm 1.38$	21/10	11
100906A	0.3–200	$1.07 \pm 0.04$	1055/132	$0.71 \pm 0.04$	$2.02 \pm 0.09$	$12.7 \pm 1.6$	348/130	707
101219B	0.1–10	$1.62 \pm 0.06$	1073/141	$0.30 \pm 0.17$	$2.41 \pm 0.08$	$0.33 \pm 0.02$	452/139	621
110106B	0.2–1000	$0.94 \pm 0.03$	228/53	$0.59 \pm 0.06$	$1.42 \pm 0.08$	$13.5 \pm 4.4$	77/51	151
110503A	0.1–1000	$1.12 \pm 0.01$	612/392	$1.05 \pm 0.01$	$1.48 \pm 0.05$	$34.4 \pm 12.2$	487/390	125
110715A	0.08–1000	$0.91 \pm 0.01$	799/256	$0.21 \pm 0.15$	$0.97 \pm 0.01$	$0.22 \pm 0.05$	606/254	193
110808A	0.4–1000	$0.67 \pm 0.04$	24/12	$0.57 \pm 0.04$	$1.41 \pm 0.33$	$167 \pm 79.1$	9/10	15
110818A <sup>b</sup>	0.5–200	$1.18 \pm 0.03$	112/59	$1.15 \pm 0.03$	$2.37 \pm 0.65$	$66.9 \pm 29.7$	99/57	13
111008A	0.3–1000	$0.88 \pm 0.03$	928/136	$0.29 \pm 0.05$	$1.30 \pm 0.03$	$7.42 \pm 1.10$	203/134	725
111123A	4–200	$1.08 \pm 0.05$	124/42	$0.73 \pm 0.09$	$1.93 \pm 0.21$	$34.9 \pm 10.1$	56/40	68
111129A	0.1–350	$0.87 \pm 0.03$	212/46	$0.47 \pm 0.12$	$1.23 \pm 0.05$	$2.93 \pm 1.43$	65/44	147
111228A	0.4–1000	$0.88 \pm 0.02$	767/148	$0.39 \pm 0.03$	$1.25 \pm 0.03$	$12.9 \pm 1.8$	179/146	588
111229A	0.2–20	$0.34 \pm 0.11$	314/35	$-0.13 \pm 0.08$	$2.15 \pm 0.40$	$6.94 \pm 1.05$	74/33	240
120118B	0.3–100	$0.53 \pm 0.05$	160/35	$-0.50 \pm 0.17$	$1.02 \pm 0.07$	$2.31 \pm 0.34$	41/33	119
120119A <sup>b</sup>	0.15–100	$1.01 \pm 0.01$	201/91	$1.00 \pm 0.02$	$2.46 \pm 0.65$	$32.4 \pm 8.1$	180/89	21
120211A	1–100	$0.63 \pm 0.16$	92/12	$-0.25 \pm 0.19$	$1.29 \pm 0.17$	$7.71 \pm 2.07$	17/10	75
120224A	0.3–600	$0.73 \pm 0.03$	390/79	$-0.59 \pm 0.16$	$0.98 \pm 0.03$	$1.94 \pm 0.23$	115/77	275
120326A	3–1000	$0.25 \pm 0.05$	1717/193	$-0.24 \pm 0.03$	$2.04 \pm 0.07$	$51.7 \pm 1.9$	250/191	1467
120327A	0.2–200	$1.02 \pm 0.03$	259/59	$0.65 \pm 0.08$	$1.53 \pm 0.07$	$3.36 \pm 0.92$	105/57	154
120404A	0.4–200	$0.94 \pm 0.07$	175/37	$0.24 \pm 0.18$	$1.81 \pm 0.10$	$3.17 \pm 0.61$	45/35	130
120422A	1–2000	$0.63 \pm 0.08$	35/9	$0.22 \pm 0.08$	$1.21 \pm 0.14$	$153 \pm 54$	4/7	31
120521C	0.7–100	$0.62 \pm 0.12$	37/8	$0.34 \pm 0.07$	$2.68 \pm 0.64$	$22.1 \pm 3.8$	4/6	33
120811C	0.2–100	$0.87 \pm 0.02$	100/50	$0.54 \pm 0.09$	$1.16 \pm 0.10$	$3.15 \pm 1.74$	66/48	34
120907A	0.1–300	$0.89 \pm 0.02$	244/88	$0.50 \pm 0.10$	$1.10 \pm 0.04$	$2.01 \pm 0.87$	140/86	104
121024A	3–300	$1.13 \pm 0.05$	88/46	$0.83 \pm 0.14$	$1.58 \pm 0.24$	$30.2 \pm 30.2$	63/44	25
121027A	30–3000	$1.06 \pm 0.04$	246/79	$0.45 \pm 0.13$	$1.56 \pm 0.08$	$166 \pm 39$	101/77	145
121128A	0.15–100	$1.13 \pm 0.04$	656/93	$0.50 \pm 0.05$	$1.62 \pm 0.04$	$1.46 \pm 0.20$	115/91	541
121209A	0.1–60	$0.82 \pm 0.03$	383/88	$-0.67 \pm 0.19$	$1.22 \pm 0.03$	$0.87 \pm 0.11$	99/86	284
130408A	0.1–100	$0.87 \pm 0.05$	718/57	$0.28 \pm 0.33$	$1.46 \pm 0.11$	$2.51 \pm 2.16$	301/55	417
130418A	0.1–500	$1.16 \pm 0.02$	23/96	$0.72 \pm 0.10$	$1.41 \pm 0.09$	$0.68 \pm 0.34$	166/94	67
130505A	2–2000	$1.37 \pm 0.01$	557/272	$0.92 \pm 0.05$	$1.61 \pm 0.03$	$22.4 \pm 4.2$	288/270	269
130511A	0.07–40	$1.02 \pm 0.05$	65/26	$-0.70 \pm 0.59$	$1.13 \pm 0.05$	$0.18 \pm 0.03$	31/24	34
130603B <sup>c</sup>	0.04–200	$0.78 \pm 0.03$	524/76	$0.31 \pm 0.07$	$1.52 \pm 0.07$	$2.28 \pm 0.36$	155/74	69
130606A	4–300	$2.40 \pm 0.20$	1017/37	$-0.23 \pm 0.68$	$1.76 \pm 0.09$	$9.12 \pm 1.79$	38/35	979
130612A	0.7–50	$0.92 \pm 0.05$	13/11	$0.40 \pm 0.16$	$1.26 \pm 0.08$	$3.32 \pm 1.14$	2/9	11
130925A	20–10000	$1.02 \pm 0.01$	923/441	$0.75 \pm 0.04$	$1.40 \pm 0.04$	$322 \pm 66$	612/439	311
131030A	0.4–2000	$1.10 \pm 0.01$	461/264	$0.78 \pm 0.06$	$1.25 \pm 0.02$	$2.60 \pm 0.90$	344/262	117
131117A	0.2–200	$0.93 \pm 0.03$	21/14	$0.05 \pm 0.39$	$1.03 \pm 0.05$	$0.57 \pm 0.23$	10/12	11
140114A	1–300	$4.62 \pm 0.76$	16053/32	$0.17 \pm 0.10$	$1.21 \pm 0.13$	$18.8 \pm 5.8$	41/30	16012
140206A	0.5–2000	$0.99 \pm 0.01$	1598/476	$0.56 \pm 0.05$	$1.29 \pm 0.02$	$4.60 \pm 0.74$	751/474	846
140318A	0.1–100	$1.56 \pm 0.05$	256/54	$0.20 \pm 0.34$	$1.77 \pm 0.06$	$0.24 \pm 0.05$	109/52	147
140419A	0.8–2000	$1.14 \pm 0.01$	642/253	$0.72 \pm 0.07$	$1.40 \pm 0.03$	$5.47 \pm 1.26$	340/251	302
140430A	3–200	$0.75 \pm 0.04$	57/39	$0.60 \pm 0.10$	$1.53 \pm 0.43$	$47.7 \pm 22.1$	45/37	12
140506A	0.7–3000	$0.91 \pm 0.01$	246/162	$0.51 \pm 0.30$	$0.95 \pm 0.03$	$1.62 \pm 1.22$	229/160	17

Table 2 – continued

GRB	$t_1$ – $t_2$ [ks]	SPL model : $f_S(t)$		DPL model: $f_D(t)$			$\Delta\chi^2$ <sup>a</sup>	
		$\alpha_1$	$\chi^2/dof$	$\alpha_1$	$\alpha_2$	$t_b$ [ks]		$\chi^2/dof$
140512A	0.3–300	0.92 ± 0.01	1206/377	0.73 ± 0.02	1.57 ± 0.05	13.2 ± 1.6	482/375	724
140518A	0.2–20	0.79 ± 0.05	138/37	0.36 ± 0.08	1.63 ± 0.22	3.20 ± 0.72	57/35	81
140614A	5–200	1.32 ± 0.09	53/23	−0.71 ± 1.18	1.60 ± 0.13	7.42 ± 1.28	35/21	18
140629A	0.1–100	0.98 ± 0.02	466/112	0.81 ± 0.02	1.79 ± 0.08	7.72 ± 1.26	140/110	326
140703A	2–100	1.38 ± 0.06	308/73	0.57 ± 0.14	2.13 ± 0.13	13.6 ± 2.2	120/71	188
141004A	0.04–100	1.02 ± 0.07	148/24	0.67 ± 0.05	2.02 ± 0.17	3.59 ± 0.68	25/22	123
141121A	100–1000	1.22 ± 0.17	36/12	0.02 ± 0.35	2.61 ± 0.35	318 ± 46	8/10	28
141220A	0.08–40	1.16 ± 0.03	58/28	−0.29 ± 0.26	1.40 ± 0.04	0.20 ± 0.03	16/26	42
150323A	0.35–400	0.77 ± 0.06	99/21	0.52 ± 0.08	1.29 ± 0.20	17.5 ± 12.5	44/19	55
150910A	0.2–300	0.95 ± 0.02	2898/352	0.43 ± 0.03	2.25 ± 0.05	6.17 ± 0.35	694/350	2204
151021A	0.2–300	1.15 ± 0.01	279/118	0.91 ± 0.07	1.42 ± 0.05	2.67 ± 1.48	168/116	111
151027A	0.5–1000	0.93 ± 0.02	3546/453	0.06 ± 0.03	1.65 ± 0.02	3.92 ± 0.15	642/451	2904
151027B	2–500	0.89 ± 0.04	87/44	0.67 ± 0.07	1.46 ± 0.18	49.2 ± 23.3	50/42	37
151029A	0.1–30	1.09 ± 0.08	32/8	0.61 ± 0.25	1.45 ± 0.31	1.22 ± 1.38	15/6	17
151215A	0.4–200	0.99 ± 0.06	23/12	−0.09 ± 0.47	1.13 ± 0.06	1.02 ± 0.34	8/10	15
160121A	0.2–500	0.41 ± 0.04	53/24	0.29 ± 0.04	1.84 ± 0.50	18.9 ± 4.2	22/22	31
160227A	1.5–1000	0.76 ± 0.03	437/103	0.19 ± 0.08	1.11 ± 0.04	18.0 ± 3.2	172/101	265
160804A	3–1000	0.74 ± 0.04	115/45	−0.27 ± 0.44	0.92 ± 0.07	9.10 ± 2.82	76/43	39
161014A	0.1–100	0.96 ± 0.03	293/63	0.60 ± 0.08	1.82 ± 0.09	2.77 ± 0.58	92/61	201
161017A	3–1000	1.23 ± 0.03	204/83	0.86 ± 0.09	1.75 ± 0.10	27.5 ± 7.8	110/81	94
161108A	0.6–800	0.55 ± 0.04	81/26	0.34 ± 0.07	1.00 ± 0.20	63.6 ± 46.8	44/24	37
161117A	0.4–2000	0.88 ± 0.02	495/147	0.67 ± 0.04	1.24 ± 0.05	16.4 ± 5.6	258/145	237
161129A	0.2–30	0.86 ± 0.06	555/58	−0.09 ± 0.24	2.14 ± 0.09	2.30 ± 0.46	100/56	455
161219B	0.8–20000	0.81 ± 0.01	1094/396	0.53 ± 0.03	0.97 ± 0.02	35.5 ± 9.7	640/394	454
170113A	0.2–1000	0.86 ± 0.02	674/161	0.51 ± 0.04	1.26 ± 0.03	4.77 ± 0.88	227/159	447
170202A	0.3–400	0.86 ± 0.04	191/40	−0.18 ± 0.14	1.15 ± 0.05	2.00 ± 0.32	50/38	141
170519A	0.6–300	0.96 ± 0.04	309/81	0.40 ± 0.09	1.36 ± 0.08	8.30 ± 1.71	154/79	155
170531B	1–100	0.78 ± 0.06	25/12	0.43 ± 0.46	1.09 ± 0.30	5.88 ± 12.5	14/10	11
170607A	0.7–1000	0.68 ± 0.02	578/184	0.42 ± 0.03	1.07 ± 0.04	26.8 ± 6.0	237/182	341
170705A	0.7–3000	0.85 ± 0.02	870/223	0.53 ± 0.04	1.20 ± 0.04	29.8 ± 6.5	421/221	449
170714A	0.3–1000	0.91 ± 0.01	18200/1398	0.53 ± 0.02	3.76 ± 0.09	11.9 ± 0.3	7908/1396	10292
171205A	5–3000	0.65 ± 0.06	369/44	−0.27 ± 0.11	1.10 ± 0.07	91.4 ± 15.1	87/42	282
180325A	0.2–100	1.07 ± 0.03	999/114	−0.01 ± 0.17	2.05 ± 0.04	1.81 ± 0.28	138/112	861
180620B	0.5–1000	0.73 ± 0.02	392/98	0.47 ± 0.04	1.21 ± 0.08	48.9 ± 12.6	180/96	212
180624A	3–300	0.95 ± 0.07	76/34	0.51 ± 0.23	1.42 ± 0.19	15.5 ± 8.6	51/32	25

**Notes.**<sup>a</sup> A DPL model is statistically preferred at  $> 3\sigma$  over a simpler SPL model when  $\Delta\chi^2 > 10$ .<sup>b</sup> Best-fitting values of  $\alpha_1$  and  $\alpha_2$  of DPL model are consistent with the jet break (see section 5).<sup>c</sup> Short GRBs.<sup>d</sup> Events showing only X-ray flares until 3 ks after the burst trigger.<sup>e</sup> Events showing long initial steep decay phase lasting 2 ks.

**Table 3.** Best-fitting model parameters of GRBs in Sample C

GRB	$t_1-t_2$ [ks]	SPL model : $f_S(t)$		DPL model: $f_D(t)$			$\Delta\chi^2$ <sup>a</sup>	
		$\alpha_1$	$\chi^2/dof$	$\alpha_1$	$\alpha_2$	$t_b[ks]$		
Single power-law (SPL) events								
081118 <sup>e</sup>	0.9–1000	$0.60 \pm 0.05$	13/8	$0.49 \pm 0.25$	$0.77 \pm 0.75$	$138 \pm 1210$	11/6	2
090422	0.5–100	$0.94 \pm 0.03$	40/28	$-0.05 \pm 0.94$	$1.01 \pm 0.05$	$0.82 \pm 0.34$	35/26	5
090831C <sup>d</sup>	4–150	$0.84 \pm 0.06$	7/9	$-0.55 \pm 3.11$	$0.91 \pm 0.10$	$5.49 \pm 2.23$	6/7	1
091221 <sup>d</sup>	0.2–200	$1.09 \pm 0.04$	10/10	$0.99 \pm 0.61$	$1.20 \pm 0.72$	$8.3 \pm 207$	9/8	1
110801A <sup>d</sup>	0.55–100	$1.41 \pm 0.02$	411/111					< 1
Double power-law (DPL) events								
080928	3–100	$1.51 \pm 0.06$	187/72	$0.39 \pm 0.56$	$1.84 \pm 0.11$	$7.41 \pm 1.85$	145/70	42
081008	0.5–1000	$1.06 \pm 0.04$	235/53	$0.83 \pm 0.03$	$2.00 \pm 0.10$	$18.8 \pm 3.0$	49/51	186
081126	0.2–800	$0.98 \pm 0.04$	567/74	$0.45 \pm 0.07$	$1.49 \pm 0.05$	$5.11 \pm 1.26$	133/72	434
081127	0.4–50	$0.64 \pm 0.11$	35/9	$-0.53 \pm 0.50$	$1.03 \pm 0.22$	$2.05 \pm 0.94$	14/7	11
081222	0.1–100	$1.03 \pm 0.01$	654/368	$0.65 \pm 0.08$	$1.13 \pm 0.02$	$0.38 \pm 0.14$	492/366	162
090113	0.1–400	$1.10 \pm 0.04$	100/25	$0.13 \pm 0.22$	$1.28 \pm 0.05$	$0.55 \pm 0.16$	38 /23	62
090407	0.9–1000	$0.65 \pm 0.04$	599/111	$0.36 \pm 0.03$	$1.63 \pm 0.09$	$68.1 \pm 8.3$	181/109	418
090516	3–200	$1.28 \pm 0.03$	378/133	$0.65 \pm 0.10$	$1.88 \pm 0.09$	$16.5 \pm 2.6$	184/131	194
090518	0.3–100	$0.75 \pm 0.03$	72/35	$0.27 \pm 0.18$	$1.05 \pm 0.09$	$2.41 \pm 1.16$	42/33	30
090529	2–1000	$0.68 \pm 0.06$	18/8	$0.51 \pm 0.05$	$1.68 \pm 0.31$	$223 \pm 71$	3/6	15
090621A	0.8–1000	$0.92 \pm 0.03$	152/53	$0.55 \pm 0.07$	$1.27 \pm 0.06$	$10.6 \pm 3.4$	56/51	96
090728	0.3–100	$1.10 \pm 0.06$	120/26	$0.00 \pm 0.18$	$1.80 \pm 0.09$	$1.81 \pm 0.25$	23/24	97
090813	0.05–1000	$1.03 \pm 0.01$	1666/295	$0.23 \pm 0.04$	$1.25 \pm 0.01$	$0.55 \pm 0.04$	400/293	1266
091208B	0.2–1000	$0.97 \pm 0.02$	199/59	$-0.22 \pm 0.25$	$1.15 \pm 0.03$	$0.81 \pm 0.14$	86/57	113
100111A	0.1–300	$0.84 \pm 0.03$	69/33	$0.39 \pm 0.12$	$1.04 \pm 0.06$	$1.38 \pm 0.60$	35/31	34
100212A	1–100	$0.90 \pm 0.10$	50/9	$0.36 \pm 0.43$	$1.35 \pm 0.29$	$6.43 \pm 7.81$	20/7	30
100316D	0.1–1000	$0.63 \pm 0.04$	3950/402	$0.07 \pm 0.03$	$1.97 \pm 0.04$	$0.83 \pm 0.01$	529/400	3421
100418A	0.9–1000	$0.47 \pm 0.10$	294/21	$-0.18 \pm 0.07$	$1.33 \pm 0.11$	$71.5 \pm 14.6$	26/19	268
100614A	1.5–1000	$0.69 \pm 0.05$	130/30	$0.56 \pm 0.05$	$2.48 \pm 0.54$	$202 \pm 41$	65/28	65
100704A	0.5–2000	$0.92 \pm 0.02$	450/157	$0.67 \pm 0.03$	$1.32 \pm 0.05$	$33.8 \pm 8.0$	199/155	251
100725B	0.5–500	$0.87 \pm 0.04$	216/53	$0.41 \pm 0.05$	$1.41 \pm 0.07$	$16.0 \pm 2.6$	54/51	162
100728B	0.07–100	$1.04 \pm 0.02$	74/38	$0.94 \pm 0.08$	$1.66 \pm 0.35$	$6.04 \pm 5.48$	45/36	29
100802A	5–1000	$0.55 \pm 0.05$	65/22	$-0.40 \pm 0.30$	$0.72 \pm 0.07$	$23.2 \pm 9.3$	28/20	37
100902A	1.5–2000	$0.77 \pm 0.02$	144/56	$0.72 \pm 0.02$	$4.44 \pm 1.11$	$823 \pm 90$	95/54	49
101219B	0.1–10	$1.62 \pm 0.06$	1073/141	$0.30 \pm 0.17$	$2.41 \pm 0.08$	$0.33 \pm 0.02$	452/139	621
110102A	0.5–1000	$0.94 \pm 0.02$	1290/281	$0.49 \pm 0.03$	$1.41 \pm 0.03$	$13.4 \pm 1.3$	335/279	955
110223A	0.5–800	$0.60 \pm 0.03$	27/22	$0.41 \pm 0.10$	$0.79 \pm 0.10$	$23.5 \pm 33.0$	16/20	11
110411A	0.3–200	$0.86 \pm 0.04$	116/37	$0.40 \pm 0.11$	$1.24 \pm 0.10$	$3.26 \pm 1.18$	56/35	60
110414A	0.6–200	$1.18 \pm 0.07$	138/30	$0.05 \pm 0.27$	$1.65 \pm 0.08$	$2.58 \pm 0.46$	46/28	92
110808A	0.4–1000	$0.67 \pm 0.04$	24/12	$0.57 \pm 0.04$	$1.41 \pm 0.33$	$167 \pm 79$	9/10	15
120118B	0.3–100	$0.53 \pm 0.05$	160/35	$-0.50 \pm 0.17$	$1.02 \pm 0.07$	$2.31 \pm 0.34$	41/33	119

**Notes.**<sup>a</sup> A DPL model is statistically preferred at  $> 3\sigma$  over a simpler SPL model when  $\Delta\chi^2 > 10$ .<sup>b</sup> Best-fitting values of  $\alpha_1$  and  $\alpha_2$  of DPL model are consistent with the jet break (see section 5).<sup>d</sup> Events showing only X-ray flares until 3 ks after the burst trigger.<sup>e</sup> Events showing long initial steep decay phase lasting 2 ks.